Article:
Gower, A.L. orcid.org/0000-0002-3229-5451, Parnell, W.J. and Abrahams, I.D. (2019) Multiple waves propagate in random particulate materials. SIAM Journal on Applied Mathematics, 79 (6). pp. 2569-2592. ISSN 0036-1399

https://doi.org/10.1137/18M122306X

SIAM J. APPL. MATH.
Vol. 79, No. 6, pp. 2569–2592

MULTIPLE WAVES PROPAGATE IN RANDOM PARTICULATE MATERIALS*

ARTUR L. GOWER†‡, WILLIAM J. PARNELL‡, AND I. DAVID ABRAHAMS§

Abstract. For over 70 years it has been assumed that scalar wave propagation in (ensemble-averaged) random particulate materials can be characterized by a single effective wavenumber. Here, however, we show that there exist many effective wavenumbers, each contributing to the effective transmitted wave field. Most of these contributions rapidly attenuate away from boundaries, but they make a significant contribution to the reflected and total transmitted field beyond the low-frequency regime. In some cases at least *two* effective wavenumbers have the same order of attenuation. In these cases a single effective wavenumber does not accurately describe wave propagation even far away from boundaries. We develop an efficient method to calculate all of the contributions to the wave field for the scalar wave equation in two spatial dimensions, and then compare results with numerical finite-difference calculations. This new method is, to the best of the authors' knowledge, the first of its kind to give such accurate predictions across a broad frequency range and for general particle volume fractions.

Key words. wave propagation, random media, inhomogeneous media, composite materials, backscattering, multiple scattering, ensemble averaging

AMS subject classifications. 74J20, 45B05, 45E10, 82D30, 82D15, 78A48, 74A40

DOI. 10.1137/18M122306X

1. Introduction.

Materials comprising small particles, inclusions or defects, randomly distributed inside an otherwise uniform host medium, are ubiquitous. Commonly occurring examples include composites, emulsions, dense suspensions, complex gases, polymers, and foods. Understanding how electromagnetic, elastic, or acoustic waves propagate through such media is crucial to characterize these materials and also to design new materials that can control wave propagation. For example, we may wish to use wave techniques to *determine* statistical information about the material, e.g., volume fraction of particles, particle radius distribution, etc.

The exact positions of all particles are usually unknown. The common approach to deal with this, which we adopt here, is to ensemble average over such unknowns. In certain scenarios, such as light scattering [38], it is easier to measure the average intensity of the wave, but these methods often need the ensemble-averaged field as a first step [14, 54, 53].

1.1. Historical perspective.

The seminal work in this field is Foldy's 1945 paper [14], which introduced the *Foldy closure approximation* in order to deduce *a single "effective wavenumber"* k_* in the form $k_* = k_0 - \phi g$, where ϕ is the *volume fraction* of particles and g is the scattering coefficient associated with a single particle. Foldy introduced the notion of ensemble averaging the field, but the expression deduced

*Received by the editors October 25, 2018; accepted for publication (in revised form) August 6, 2019; published electronically December 17, 2019.

https://doi.org/10.1137/18M122306X

Funding: This work was supported by EPSRC (EP/M026205/1, EP/L018039/1) and by the Isaac Newton Institute for Mathematical Sciences (EP/K032208/1).

†Department of Mechanical Engineering, The University of Sheffield, Sheffield S10 2TN, UK (arturgower@gmail.com, http://arturgower.github.io).

‡School of Mathematics, University of Manchester, Oxford Road, Manchester M13 9PL, UK (william.j.parnell@manchester.ac.uk).

§Isaac Newton Institute for Mathematical Sciences, 20 Clarkson Road, Cambridge CB3 0EH, UK (i.d.abrahams@newton.ac.uk).

for k_* was restricted to dilute dispersions and isotropic scattering. Lax improved on this by incorporating a higher-order closure approximation [25, 26], now known as the *quasi-crystalline approximation* (QCA), and by including pair-correlation functions, which represent particle distributions. Both QCA and pair-correlations have now been extensively used in multiple scattering theory. The most commonly used pair-correlation is *hole-correction* [13]. Both QCA and hole-correction are examples of statistical closure approximations [2, 3], which are techniques widely used in statistical physics. For multiple scattering, the accuracy of these approximations has been supported by theoretical [33, 34], numerical [9], and experimental [59, 67] evidence. These approximations also make no explicit assumptions on the frequency range, material properties, or particle volume fraction. We note, however, that to the best of our knowledge, there are no rigorous bounds for the error introduced by these approximations. For a brief discussion on these approximations see [21].

For an overview of the literature on multiple scattering in particulate materials, making use of closure approximations, see the books [55, 31, 38]. We now briefly summarize how calculating effective wavenumbers has evolved since the early work of Foldy and Lax.

Over the last 60 years, corrections to the dilute limit have been sought, mainly by expanding in the volume fraction ϕ and then attempting to determine the $\mathrm{O}(\phi^2)$ contribution to k_*. Twersky [56] obtained an expression for this contribution as a function of $f(\pi - 2\theta_{\mathrm{inc}})$ and $f(0)$, where θ_{inc} is the angle of incidence of an exciting plane wave (see Figure 1), and $f(\theta)$ is the far field scattering pattern from one particle [28]. The dependence on θ_{inc} implies that k_* depends on the angle of incidence, which is counterintuitive. Waterman and Truell [63] obtained the same expression as Twersky but with $\theta_{\mathrm{inc}} = 0$. However, [63] used a "slab pair-correlation function" that (theoretically) limits the validity of their approach to dilute dispersions (small ϕ); see [27] for comparisons with experiments, and see [5] for a discussion in two dimensions. Extensions that incorporate the hole-correction pair-correlation function were described by Fikioris and Waterman [13]. The Waterman and Truell expressions for three-dimensional elasticity are written down in [68, 45]. Work in two-dimensional elasticity using QCA was reported by [8]. Lloyd and Berry [30] calculated the $\mathrm{O}(\phi^2)$ contribution by including both QCA and hole-correction for the scalar wave equation, although the language used stemmed from nuclear physics. More recently, [28, 29] rederived the Lloyd and Berry formula for the effective wavenumber without appealing to the so-called extinction theorem used in many previous papers, such as [60], and without recourse to "resumming series." The work was then extended in order to calculate effective reflection and transmission in [32]. Gower et al. [21] subsequently extended this result to model multispecies materials, i.e., to account for polydisperse distributions.

Other related work on effective wavenumbers and attenuation include comparing the properties of single realizations to those of effective waves [49, 6, 7, 40], and effective waves in polycrystals [50, 64] such as steel and ceramics. The polycrystal papers use a similar framework to waves in particulate materials, except they assume weak scattering which excludes multiple scattering.

1.2. Overview of this paper. A common *assumption* used across the field of random particulate materials, including those mentioned above, is to assume that there exists a *single, unique, complex effective wavenumber* k_* that characterizes the material. For example, for an incident wave $\mathrm{e}^{\mathrm{i}kx - \mathrm{i}\omega t}$, of fixed frequency ω, exciting a half-space (see Figure 1) filled with particles, the tacit assumption is that the

ensemble-averaged wave $\langle u(x)\rangle$ travelling inside the particulate material takes the form

$$\langle u(x)\rangle = a\mathrm{e}^{\mathrm{i}kx-\mathrm{i}\omega t} + b_*\mathrm{e}^{\mathrm{i}k_*x-\mathrm{i}\omega t}. \tag{1.1}$$

See [32] for a brief derivation. This assumption has been widely used in acoustics [28, 29, 31, 12], elasticity [61, 42, 43, 46, 10] (including thermo-viscous effects), electromagnetism [58, 59, 52], and even quantum waves [51]. For example, it is a key step in deducing radiative transfer equations from first principles [35, 37].

In this work, we show, however, that there *does not exist a single, unique* effective wavenumber. Instead an infinite number of effective wavenumbers $k_1, k_2, k_3, \ldots$ exist, so that the average field inside the particulate material takes the form

$$\langle u(x)\rangle = ae^{ikx-i\omega t} + \sum_{p=1}^{\infty} b_p e^{ik_p x-i\omega t}. \tag{1.2}$$

In many scenarios, the majority of these waves are highly attenuating, i.e., k_p has a large imaginary part for $p > 1$. In these cases, the least attenuating wavenumber k_1 will dominate the transmitted field in $\langle u(x)\rangle$, and k_1 will often be given by classical multiple scattering theory, as discussed in subsection 1.1. However, these other effective waves can still have a significant contribution to the reflected (backscattered) wave from a random particulate material, especially at higher frequencies and beyond the low volume fraction limit. Furthermore, there are scenarios where there are at least two effective wavenumbers, say k_1 and k_2, with the same order of attenuation. In these cases using only one effective wavenumber, k_1 or k_2, is insufficient to accurately calculate $\langle u(x)\rangle$, even for x far away from the interface between the homogeneous and particular materials.

We examine the simplest case that exhibits these multiple waves—two spatial dimensions (x, y) for the scalar wave equation—and consider particles placed in the half-space $x > 0$, which reflects incoming waves. We not only demonstrate that there are multiple effective wavenumbers, but we also use them to develop a highly accurate method to calculate $\langle u(x)\rangle$ and the reflection coefficient. This method agrees extremely well with numerical solutions, calculated using a finite-difference method, but is more efficient. We provide software [17] that implements the methods presented and reproduce the results of this paper.

In a separate paper [18], we develop a *proof* that (1.2) is the analytical solution for the ensemble-averaged wave. However, the proof in [18] is not constructive, in contrast to the work presented here, where we present a method that determines all effective waves (1.2).

We begin by deducing the governing equation for ensemble-averaged waves in section 2. In section 3 we then show that multiple effective wavenumbers exist. To calculate these effective wavenumbers, we need to match them to the field near the interface at $x = 0$, which leads us to develop a discrete solution in section 4. The discrete solution also serves as the basis for a numerical method, which we use later as a benchmark. In section 5 we develop the matching method, which incorporates all of the effective waves. In section 6 we summarize the fields and reflection coefficients calculated by the matching method, the numerical method, and existing methods used in the literature. We subsequently compare their results in section 7. In section 8 we summarize the main results of the paper and discuss future work.

2. Ensemble-averaged multiple scattering. Consider a region $\mathcal{R}$ filled with N particles or inclusions that are uniformly distributed. The field u is governed by

the scalar wave equations:

$$\nabla^2 u + k^2 u = 0 \quad \text{(in the background material)}, \tag{2.1}$$

$$\nabla^2 u + k_o^2 u = 0 \quad \text{(inside a particle)}, \tag{2.2}$$

where k and k_o are the real wavenumbers of the background and inclusion materials, respectively. For the sake of simplicity, we assume all particles are the same, except for their position and rotation about their center. For a distribution of particles, or multi-species, see [21].

In two dimensions, any incident wave[1] v_j and scattered wave u_j can be written in the form

$$v_j(r_j, \theta_j) = \sum_{n=-\infty}^{\infty} v_{nj} \mathrm{J}_n(kr_j) \mathrm{e}^{\mathrm{i}n\theta_j}, \tag{2.3}$$

$$u_j(r_j, \theta_j) = \sum_{n=-\infty}^{\infty} u_{nj} \mathrm{H}_n(kr_j) \mathrm{e}^{\mathrm{i}n\theta_j}, \tag{2.4}$$

with (r_j, θ_j) being the polar coordinates of $\mathbf{x} - \mathbf{x}_j$, where $\mathbf{x}_j = (x_j, y_j)$ is a vector pointing to the center of the jth particle, from some suitable origin, and $\mathbf{x}$ is any vector; see Figure 1. The J_n and H_n are, respectively, Bessel and Hankel functions of the first kind. The representation (2.4) is valid when r_j is large enough for (r_j, θ_j) to be outside of the jth particle for all θ_j. For example, in Figure 1 this distance would be $r_j > a_o$.

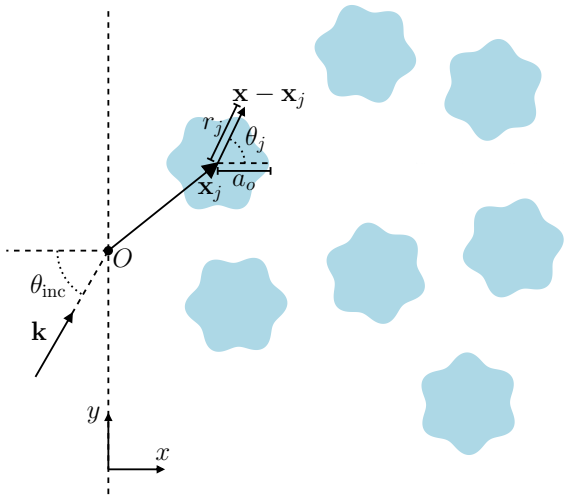

FIG. 1. *Coordinates for particles with the origin O. The particles are only placed in $x > 0$, that is, to the right of the dashed line. The vector $\mathbf{k} = k(\cos\theta_{\text{inc}}, \sin\theta_{\text{inc}})$ shows the direction of the incident plane wave.*

The T-matrix is a linear operator, in the form of an infinite matrix, such that

$$u_{nj} = \sum_{m=-\infty}^{\infty} T_{nm}(\tau_j) v_{mj} \quad \text{for } n = -\infty, \ldots, \infty \text{ and } j = 1, \ldots, N, \tag{2.5}$$

[1]Equation (2.3) assumes that the incident wave originates outside of the jth particle, which is normally the case.

where we recall that N is the number of particles. The angle τ_j gives the particles' rotation about their center $\boldsymbol{x}_j$. Allowing particles to have different rotations, and assuming all $\tau_j \in [0, 2\pi]$ to be equally likely, will lead to ensemble-averaged equations that are equivalent to the equations for circular particles [39]. This matrix $\mathbf{T}$ exists when scattering is a linear operation (elastic scattering), and can accommodate particles with a large variety of shapes and properties [15, 16, 62]; it is especially useful for multiple scattering [61, 39, 19].

The T-matrix also accounts for the particles' boundary conditions. For instance, if u represents pressure, ρ and c are the background density and wave speed, and the particles are circular with density ρ_o, sound-speed c_o, and radius a_o, then continuity of pressure and displacement across the particles' boundary [28, section IV A] yields

$$T_{nm} = -\delta_{nm} Z_o^m, \quad \text{with} \quad Z_o^m = \frac{q_o J_m'(ka_o) J_m(k_o a_o) - J_m(ka_o) J_m'(k_o a_o)}{q_o H_m'(ka_o) J_m(k_o a_o) - H_m(ka_o) J_m'(k_o a_o)}, \tag{2.6}$$

where $q_o = (\rho_o c_o)/(\rho c)$ and $k_o = \omega/c_o$. In this case the T-matrix is independent of the rotation τ_j.

In this paper we consider the incident plane wave

$$u_{\text{inc}}(x, y) = \mathrm{e}^{\mathrm{i}k(x\cos\theta_{\text{inc}} + y\sin\theta_{\text{inc}})} \quad \text{for} \quad \theta_{\text{inc}} \in (-\pi/2, \pi/2), \tag{2.7}$$

which excites N particles, resulting in scattered waves of the form (2.4). See Figure 1 for an illustration. The total wave u, measured outside of all particles at $\mathbf{x} = (x, y)$, is the sum of all scattered waves plus the incident wave:

$$u(x, y) = u_{\text{inc}}(x, y) + \sum_{j=1}^{N} u_j(r_j, \theta_j). \tag{2.8}$$

To reach an equation for the coefficients u_{nj} we write the total wave field incident on the jth particle v_j (2.3) as a combination of the incident wave plus the waves scattered by the other particles: $v_j(r_j, \theta_j) = u_{\text{inc}}(x, y) + \sum_{i \neq j} u_i(r_i, \theta_i)$. By then applying the Jacobi–Anger expansion to $u_{\text{inc}}(x, y)$, using Graf's addition theorem [31, 1], multiplying both sides by T_{qn}, summing over n, and then using (2.5), we obtain

$$u_{qj} = u_{\text{inc}}(x_j, y_j) \sum_{n=-\infty}^{\infty} T_{qn}(\tau_j) \mathrm{e}^{\mathrm{i}n(\pi/2 - \theta_{\text{inc}})} + \sum_{i \neq j} \sum_{m,n=-\infty}^{\infty} u_{mi} T_{qn}(\tau_j) F_{m-n}(k\boldsymbol{x}_i - k\boldsymbol{x}_j), \tag{2.9}$$

for all integers q and $j = 1, 2, \ldots, N$, where

$$F_n(\mathbf{X}) = (-1)^n \mathrm{e}^{\mathrm{i}n\Theta} H_n(R), \tag{2.10}$$

and (R, Θ) are the polar coordinates of $\mathbf{X}$.

2.1. Ensemble averaging. In practice the exact position of the particles is unknown, so rather than determine the scattering from an exact configuration of particles, we ensemble average the field u over all possible particle rotations and positions in $\mathcal{R}$. Sensing devices naturally perform ensemble averaging due to their size or from time averaging [36]. See [14, 45, 21] for an introduction to ensemble averaging of multiple scattering.

For simplicity, we assume the particle positions are independent of particle rotations, so that the probability of the particles being centered at $\mathbf{x}_1, \mathbf{x}_2, \ldots, \mathbf{x}_N$ is given by the probability density function $p(\mathbf{x}_1, \mathbf{x}_2, \ldots, \mathbf{x}_N)$. Hence, it follows that

$$\int p(\mathbf{x}_1)\mathrm{d}\mathbf{x}_1 = \int\int p(\mathbf{x}_1, \mathbf{x}_2)\mathrm{d}\mathbf{x}_1\mathrm{d}\mathbf{x}_2 = \cdots = 1, \tag{2.11}$$

where each integral is taken over $\mathcal{R}$. Further, we have

$$p(\mathbf{x}_1, \ldots, \mathbf{x}_N) = p(\mathbf{x}_j)p(\mathbf{x}_1, \ldots, \mathbf{x}_N|\mathbf{x}_j), \tag{2.12}$$

where $p(\mathbf{x}_1, \ldots, \mathbf{x}_N|\mathbf{x}_j)$ is the conditional probability density of having particles centered at $\mathbf{x}_1, \ldots, \cancel{\mathbf{x}_j}, \ldots, \mathbf{x}_N$ (not including $\mathbf{x}_j$), given that the jth particle is centered at $\mathbf{x}_j$. Given some function $F(\mathbf{x}_1, \ldots, \mathbf{x}_N)$, we denote its *ensemble average* (over particle positions) by

$$\langle F\rangle = \int \ldots \int F(\mathbf{x}_1, \ldots, \mathbf{x}_N)p(\mathbf{x}_1, \ldots, \mathbf{x}_N)\mathrm{d}\mathbf{x}_1 \ldots \mathrm{d}\mathbf{x}_N. \tag{2.13}$$

If we fix the location of the jth particle, $\mathbf{x}_j$, and average over the positions of the other particles, we obtain a *conditional average* of F given by

$$\langle F\rangle_{\mathbf{x}_j} = \int \ldots \int F(\mathbf{x}_1, \ldots, \mathbf{x}_N)p(\mathbf{x}_1, \ldots, \mathbf{x}_N|\mathbf{x}_j)\mathrm{d}\mathbf{x}_1 \ldots \cancel{\mathrm{d}\mathbf{x}_j} \ldots \mathrm{d}\mathbf{x}_N. \tag{2.14}$$

We assume that one particle is equally likely to be centered anywhere in $\mathcal{R}$, when the position of the other particles is unknown:

$$p(\mathbf{x}_j) = \frac{\mathfrak{n}}{N} \quad \text{for } \mathbf{x}_j \in \mathcal{R}, \tag{2.15}$$

where we define the number density $\mathfrak{n} = N/|\mathcal{R}|$ and the area of $\mathcal{R}$ as $|\mathcal{R}|$.

Using the above we can express $\langle u(x, y)\rangle$, for (x, y) outside of the region $\mathcal{R}$, by taking the ensemble average of both sides of (2.8) to obtain

$$\langle u(x, y)\rangle = u_{\mathrm{inc}}(x, y) + \sum_{j=1}^{N} \int_{\mathcal{R}} \langle u_j(r_j, \theta_j)\rangle_{\mathbf{x}_j} p(\mathbf{x}_j)\mathrm{d}\mathbf{x}_j \tag{2.16}$$

$$= u_{\mathrm{inc}}(x, y) + \mathfrak{n} \int_{\mathcal{R}} \langle u_1(r_1, \theta_1)\rangle_{\mathbf{x}_1} \mathrm{d}\mathbf{x}_1 \quad \text{for } \mathbf{x} \notin \mathcal{R}, \tag{2.17}$$

where we assumed that all particles are identical (apart from their position and rotation). We also used equations (2.12), (2.15) and averaged both sides over particle rotations. Using the scattered field (2.4), we then reach

$$\langle u_1(r_1, \theta_1)\rangle_{\mathbf{x}_1} = \sum_{n=-\infty}^{\infty} \langle u_{n1}\rangle_{\mathbf{x}_1} H_n(kr_1)\mathrm{e}^{\mathrm{i}n\theta_1}. \tag{2.18}$$

The simplest scenario is the limit when the particles occupy the half-space $x_1 > 0$ [28], that is, $\mathcal{R} = \{(x, y)|x > 0\}$. We focus on this case, although the method we present can be adapted to any region $\mathcal{R}$. In the limit of $\mathcal{R}$ tending to a half-space, we let $N \to \infty$ while $\mathfrak{n}$ remains fixed. Due to the symmetry between the incident wave (2.7) and the half-space $x_1 > 0$, the field $\langle u_{n1}\rangle_{\mathbf{x}_1}$ has a translational symmetry along y_1, which allows us to write [21]

$$\langle u_{n1}\rangle_{\mathbf{x}_1} = \mathcal{A}_n(kx_1)\mathrm{e}^{\mathrm{i}ky_1 \sin\theta_{\mathrm{inc}}}. \tag{2.19}$$

For step-by-step details on deriving a governing equation for $\mathcal{A}_n(kx_1)$, see [28, 10, 21]. Here we only give an overview. First multiply by $p(\boldsymbol{x}_2,\dots,\boldsymbol{x}_N|\boldsymbol{x}_1)$ on both sides of (2.9), set $j=1$, ensemble average over all particle rotations[2] and particle positions in $x>0$, and then use the statistical assumptions *hole-correction*[3] and the quasicrystalline approximation to reach the system:

$$\sum_{n=-\infty}^{\infty} \mathfrak{n} \int_{\substack{x_2>0 \\ \|\mathbf{x}_1-\mathbf{x}_2\|>a_{12}}} T_m \mathcal{A}_n(kx_2) \mathrm{e}^{\mathrm{i}k(y_2-y_1)\sin\theta_{\mathrm{inc}}} F_{n-m}(k\mathbf{x}_2 - k\mathbf{x}_1)\mathrm{d}\mathbf{x}_2 - \mathcal{A}_m(kx_1) + \mathrm{e}^{\mathrm{i}kx_1\cos\theta_{\mathrm{inc}}} T_m \mathrm{e}^{\mathrm{i}m(\pi/2-\theta_{\mathrm{inc}})} = 0 \quad \text{for} \quad x_1>0, \tag{2.20}$$

where $T_m\delta_{mq} = (2\pi)^{-1}\int_0^{2\pi} T_{mq}(\tau)\mathrm{d}\tau$, $\delta_{mq}=1$ if $m=q$ and 0 otherwise, and a_{12} is the minimum allowed distance between the center of any two particles. That is, a_{12} is at least twice the radius for circular particles. For the case shown in Figure 1 we could choose $a_{12}=2a_o$. This minimum distance a_{12} guarantees that particles do not overlap.

When the T-matrix $\mathbf{T}$ is known, we can determine the field $\mathcal{A}_n$ from the system (2.20). The aim of this paper is to efficiently solve for $\mathcal{A}_n$ and in the process reveal that $\mathcal{A}_n$ is composed of a series of effective waves.

For the rest of the paper we employ the nondimensional variables

$$X_1 = kx_1, \quad X_2 = kx_2, \quad R_o\gamma = ka_{12}, \quad \phi = \pi\mathfrak{n}\frac{R_o^2}{k^2} = \pi\mathfrak{n}\frac{a_{12}^2}{\gamma^2}, \tag{2.21}$$

where R_o is the particles' nondimensional maximum radius (in Figure 1, $R_o=ka_o$), $\gamma\geq 2$ is a chosen closeness constant, with $\gamma=2$ implying that particles can touch, and ϕ is the particle volume fraction.[4] Using nondimensional parameters helps to formulate robust numerical methods and to explore the parameter space.

3. Effective waves. An elegant way to approximate $\mathcal{A}_n$ is to assume it is a plane wave of the form [31]

$$\mathcal{A}_n(X) = \mathrm{i}^n\mathrm{e}^{-\mathrm{i}n\varphi}A_n\mathrm{e}^{\mathrm{i}XK\cos\varphi} \quad \text{for} \quad X>\bar{X}, \tag{3.1}$$

where K is the nondimensional effective wavenumber (kK is the dimensional effective wavenumber), with $\mathrm{Im}\ K\geq 0$ to be physically reasonable, the factor $\mathrm{i}^n\mathrm{e}^{-\mathrm{i}n\varphi}$ is for later convenience, and $\bar{X}$ is a length-scale we will determine later. We also restrict the complex angle φ by imposing that $-\pi/2<\mathrm{Re}\,\varphi<\pi/2$ and using

$$K\sin\varphi = \sin\theta_{\mathrm{inc}}, \tag{3.2}$$

which is due to the translational symmetry of equation (2.20) in y_1; see [21, equation (4.4)]. This relation is often called Snell's law.

As the material has been homogenized, it is tempting to make assumptions that are valid for homogeneous materials, such as assuming that only one plane wave (3.1)

[2]We assume that every particle is equally and independently likely to be rotated by any angle τ_j, which makes the ensemble-averaged T-matrix diagonal [57, 39].

[3]The assumption hole-correction is not appropriate for long and narrow particles. More generally, the method we present can be applied to any pair correlations that depend only on interparticle distance.

[4]For noncircular particles, ϕ is slightly larger than the actual particle volume fraction because we use the outer radius R_o (a_o in Figure 1) instead of the appropriate average radius.

is transmitted into the material. When the particles are very small in comparison to the wavelength, this is asymptotically correct [44], but in all other regimes this is not valid, especially close to the edge $\bar{X} = 0$, as we show below.

By substituting the ansatz (3.1) into (2.20), using (2.21) (see section SM1 in the supplementary material for details), and by restricting $X_1 > \bar{X} + \gamma R_o$, we obtain

$$\sum_{n=-\infty}^{\infty} M_{mn}(K) A_n = 0, \quad M_{mn}(K) = -R_o^2 \delta_{mn} + 2\phi T_m \frac{\mathcal{N}_{n-m}(K)}{1-K^2}, \tag{3.3}$$

$$2\phi \sum_{n=-\infty}^{\infty} \mathrm{e}^{\mathrm{i}n\theta_{\mathrm{inc}}} A_n \mathrm{e}^{-\mathrm{i}n\varphi} \frac{\mathrm{e}^{\mathrm{i}(K\cos\varphi - \cos\theta_{\mathrm{inc}})\bar{X}}}{K\cos\varphi - \cos\theta_{\mathrm{inc}}} = \mathrm{i}\pi R_o^2 \cos\theta_{\mathrm{inc}} + g(\bar{X}), \tag{3.4}$$

$$g(\bar{X}) = 2\phi \sum_{n=-\infty}^{\infty} \mathrm{e}^{\mathrm{i}n\theta_{\mathrm{inc}}} (-\mathrm{i})^{n-1} \int_0^{\bar{X}} \mathcal{A}_n(X_2) \mathrm{e}^{-\mathrm{i}X_2 \cos\theta_{\mathrm{inc}}} \mathrm{d}X_2, \tag{3.5}$$

where

$$\mathcal{N}_n(K) = \gamma R_o (H_n'(\gamma R_o) J_n(\gamma K R_o) - K H_n(\gamma R_o) J_n'(\gamma K R_o)), \tag{3.6}$$

and (3.4) is often called the extinction theorem, though we will refer to it as the extinction equation.

Using (3.3) we can calculate K by solving

$$\det(M_{mn}(K)) = 0; \tag{3.7}$$

then *the standard approach* to calculate A_n is to use $(3.3)_1$ and (3.4) and take $\bar{X} = 0$, which avoids the need to know $\mathcal{A}_n$ or to calculate $g(\bar{X})$. It is commonly assumed that there is only one viable K when fixing all the material parameters, including the incident wavenumber k. However, in general (3.7) admits many solutions, which we denote as $K = K_1, K_2, \ldots$; see Figure 2 for some examples. We order these wavenumbers so that $\mathrm{Im}\, K_p$ increases with p. There is no reason why these wavenumbers are not physically viable. Therefore we write $\mathcal{A}_n$ as a sum of effective waves:

$$\mathcal{A}_n(X) = \mathrm{i}^n \sum_{p=1}^{P} \mathrm{e}^{-\mathrm{i}n\varphi_p} A_n^p \mathrm{e}^{\mathrm{i}XK_p\cos\varphi_p} \quad \text{for } X > \bar{X}, \tag{3.8}$$

where there are an infinite number of these effective wavenumbers [18], but to reach an approximate method we need only a finite number P. Technically, (3.8) is a solution to (2.20) for $X > 0$, that is, we could take $\bar{X} = 0$. However, in this case, we found that close to $X = 0$ a very large number of effective waves P would be required to achieve an accurate solution. This is why we only use the sum of plane waves (3.8) for $X > \bar{X} > 0$.

One of these effective wavenumbers, in most cases the lowest attenuating K_1, can be calculated using an asymptotic expansion for low ϕ [28] and assuming it is a perturbation away from 1 (the background wavenumber).

Substituting (3.8) into (2.20) leads to the same dispersion equations (3.3) and (3.7), but with K_1 and A_n^1 replaced with K_p and A_n^p, which leads to

$$\sum_{n=-\infty}^{\infty} M_{mn}(K_p) A_n^p = 0 \quad \text{and} \quad \det(M_{mn}(K_p)) = 0, \tag{3.9}$$

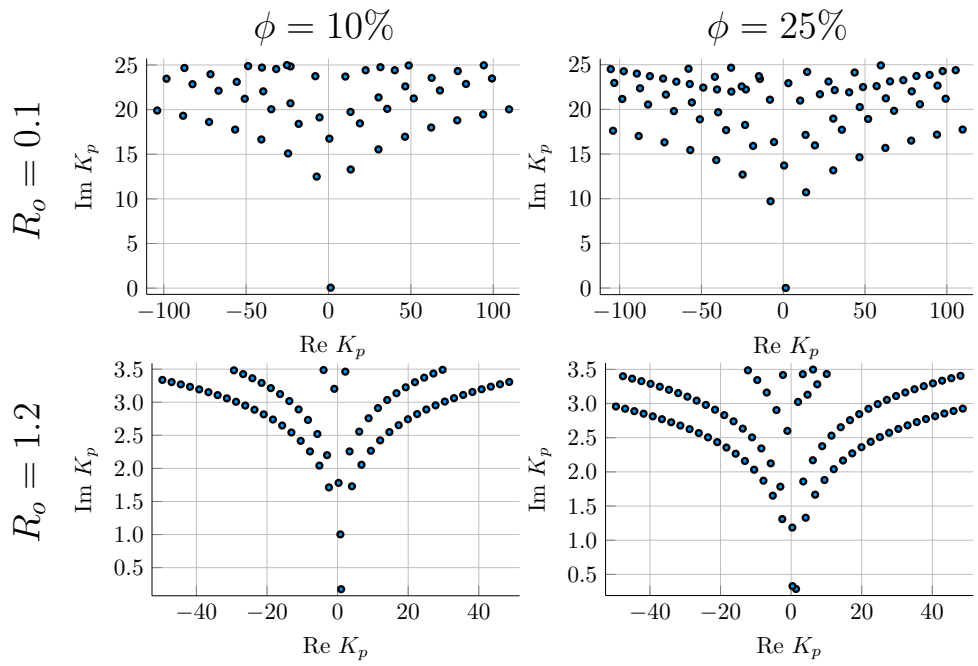

FIG. 2. *An example of the effective wavenumbers $K_1, K_2, \ldots$ that satisfy $(3.9)_2$. The particles chosen are moderately strong scatterers, with T-matrix (2.6), parameters $k = 1$, $k_o = 2.0$, $c_o = \rho_o = 0.5$, $c = \rho = 1.0$, and the nondimensional radius R_o is 0.2 for the top two graphs and 1.2 for the bottom two graphs. Note that the bottom right graph shows two wavenumbers, almost on top of each other, both with imaginary part less than 0.5.*

while for the extinction equation (3.4) we need to substitute K for K_p, φ for φ_p, and then sum over p only on the left-hand side to arrive at

$$2\phi \sum_{p=1}^{P} \sum_{n=-\infty}^{\infty} A_n^p \mathrm{e}^{\mathrm{i}n(\theta_{\mathrm{inc}}-\varphi_p)} \frac{\mathrm{e}^{\mathrm{i}(K_p \cos\varphi_p - \cos\theta_{\mathrm{inc}})\bar{X}}}{K_p \cos\varphi_p - \cos\theta_{\mathrm{inc}}} = \mathrm{i}\pi R_o^2 \cos\theta_{\mathrm{inc}} + g(\bar{X}); \tag{3.10}$$

for details see section SM1. The question now arises: how do we calculate the unknowns A_n^p? Once each K_p and φ_p are determined from $(3.9)_2$ and (3.2), then $(3.9)_1$ can be used to write the vector $\mathbf{A}^p = [\ldots, A_{-n}^p, A_{1-n}^p, \ldots, A_{n-1}^p, A_n^p, \ldots]$ in the form

$$\mathbf{A}^p = \alpha^p \mathbf{a}^p \quad \text{and} \quad \boldsymbol{\alpha} = [\alpha^1, \alpha^2, \ldots], \tag{3.11}$$

where the $\mathbf{a}^p$ are determined from $(3.9)_1$. However, only (3.10) remains to determine the vector $\boldsymbol{\alpha}$. As there is more than one effective wave, $P > 1$, (3.10) is not sufficient to determine $\boldsymbol{\alpha}$. This is because satisfying (3.9) and (3.10) only implies that the effective field (3.8) solves (2.20) for $X_1 > \bar{X} + \gamma R_o$. The missing information, needed to determine $\boldsymbol{\alpha}$, will come from solving (2.20) for $0 \le X_1 < \bar{X} + \gamma R_o$. We choose to do this by calculating a discrete solution for $\mathcal{A}_n$ within $0 \le X_1 < \bar{X} + \gamma R_o$, and then matching the $\mathcal{A}_n$ with the effective waves (3.8). The final result will be a (small) linear system (5.5).

4. A one-dimensional integral equation. Due to the symmetry between the half-space and the incident wave, we can reduce (2.20) to a one-dimensional Wiener–

Hopf integral equation:

$$\sum_{n=-\infty}^{\infty} \frac{\phi}{\pi R_o^2} \int_0^{\infty} T_m \mathcal{A}_n(X_2)\psi_{n-m}(X_2 - X_1)\mathrm{d}X_2 - \mathcal{A}_m(X_1) = -\mathrm{e}^{\mathrm{i}X_1 \cos\theta_{\mathrm{inc}}} T_m \mathrm{e}^{\mathrm{i}m(\pi/2-\theta_{\mathrm{inc}})} \quad \text{for } X_1 > 0, \tag{4.1}$$

where

$$\psi_n(X) = S_n(X) + \chi_{\{|X|<R_o\gamma\}}(B_n(X) - S_n(X)),$$

with $\chi_{\{\mathrm{true}\}} = 1$ and $\chi_{\{\mathrm{false}\}} = 0$, $S_n(X)$ is given by (A.2), and $B_n(X)$ is given by (A.6).

Kristensson [23] deduced a similar one-dimensional integral equation for electromagnetism, and in [18] we showed that the analytic solution to (4.1) is a sum of effective plane waves.

We will use (4.1) to determine the effective waves (3.8) and to formulate a completely numerical solution to (2.20), which we use as a benchmark.

4.1. The discrete form. The simplest discrete solution of (4.1) is to use a regular spaced finite-difference method and a finite-section approximation.[5] A similar finite-difference solution was used in [22].

Let $\mathcal{A}_n^j = \mathcal{A}_n(X^j)$ for $X^j = jh$ and $j = 0, \ldots, J$, with analogous notation for the other fields. We also define the vectors

$$\boldsymbol{\mathcal{A}}_n = [\mathcal{A}_n^0, \mathcal{A}_n^1, \ldots, \mathcal{A}_n^J], \quad \boldsymbol{b}_n = -\mathrm{e}^{\mathrm{i}n(\pi/2-\theta_{\mathrm{inc}})} T_n [\mathrm{e}^{\mathrm{i}X^0 \cos\theta_{\mathrm{inc}}}, \ldots, \mathrm{e}^{\mathrm{i}X^J \cos\theta_{\mathrm{inc}}}]. \tag{4.2}$$

For implementation purposes, we consider all vectors to be column vectors. We also use the block matrix $\mathbb{A}$ with components $\mathbb{A}_{n1} = \boldsymbol{\mathcal{A}}_n$, that is,

$$\mathbb{A} = [\ldots, \boldsymbol{\mathcal{A}}_{-n}, \boldsymbol{\mathcal{A}}_{1-n}, \ldots, \boldsymbol{\mathcal{A}}_n, \boldsymbol{\mathcal{A}}_{n+1}, \ldots], \tag{4.3}$$

so $\mathbb{A}$ can be viewed as a one-column matrix. The goal is to solve for $\mathbb{A}$.

To discretize the integrals in (4.1), we use $\int f(X)dX \approx \sum_j f(X^j)\sigma_j$, which in the simplest form is $\sigma_j = h$ for every j. Discretizing the integrals in (4.1), then substituting (4.2), and letting $X_1^j = X_2^j = jh$ for $j = 0, 1, \ldots, J$ leads to

$$\sum_n (\mathcal{E}_{nm}^{\ell} + \mathcal{R}_{nm}^{\ell}) - \mathcal{A}_m^{\ell} + \sum_n \sum_{j=0}^{J} Q_{mn}^{\ell j} \mathcal{A}_n^j = b_m^{\ell} \quad \text{for } \ell = 0, 1, \ldots, J, \tag{4.4}$$

where $q = \lfloor R_o\gamma/h \rfloor$,

$$Q_{mn}^{\ell j} = \frac{\phi T_m}{\pi R_o^2} \sigma_j S_{n-m}^{j-\ell} + \frac{\phi T_m}{\pi R_o^2} \sigma_{\ell j} (B_{n-m}^{j-\ell} - S_{n-m}^{j-\ell}) \chi_{\{|j-\ell|\le q\}}, \tag{4.5}$$

$$\mathcal{E}_{nm}^{\ell} = \frac{\phi T_m}{\pi R_o^2} \int_{X_2 \ge X^J} \mathcal{A}_n(X_2) S_{n-m}(X_2 - X^{\ell}) dX_2, \tag{4.6}$$

$$\mathcal{R}_{nm}^{\ell} = \chi_{\{\ell > J-q\}} \frac{\phi T_m}{\pi R_o^2} \times \int_{X^J}^{X^{\ell}+R_o\gamma} \mathcal{A}_n(X_2)(B_{n-m}(X_2 - X^{\ell}, k) - S_{n-m}(X_2 - X^{\ell}))dX_2. \tag{4.7}$$

[5] The kernel in (2.20) does not satisfy the technical requirements in [11], and we have been unable to find convergence results for approximating equations of the form (2.20). See [4] for a review on solvability.

The $\sigma_{\ell j}$ depend on ℓ because the discrete domain of integration $|j-\ell| \le q$ changes with ℓ, though the simplest choice would still be $\sigma_{\ell j} = h$.

If we did not include $\mathcal{E}^{\ell}_{nm}$ and $\mathcal{R}^{\ell}_{nm}$, then the solution of (4.4) would represent the average wave in the layer $0 \le X \le X^J$. One method to calculate the solution for the whole half-space $X \ge 0$ is to extend X^J until $\mathcal{A}_n(X^J)$ tends to zero. However, it is more computationally efficient to calculate $\mathcal{E}^{\ell}_{nm}$ and $\mathcal{R}^{\ell}_{nm}$ by approximating $\mathcal{A}_n(X)$ as a sum of plane waves, as shown below.

5. Matching the discrete form and effective waves. Here we formulate a system to solve for the unknown effective wave amplitudes α^p (3.11) and $\mathbb{A}$ (4.3). To do this, we substitute $\mathcal{A}_n(X_2)$ for the effective waves (3.8) in $\mathcal{E}^{\ell}_{nm}$ and $\mathcal{R}^{\ell}_{nm}$, (4.6) and (4.7), and we calculate the integral $g(\bar{X})$ in (3.10) by substituting $\mathcal{A}_n(X_2)$ for the discrete solution $\mathcal{A}^j_n$ (4.2). Finally, to determine the α^p, and therefore the effective waves (3.8), we impose that (3.8) matches the discrete solution (4.2) in a thin layer near the boundary $\bar{X}$. For an illustration see Figure 3. Imposing this match acts like a boundary condition for the effective waves. From here onwards we assume that $\bar{X} = X^L$.

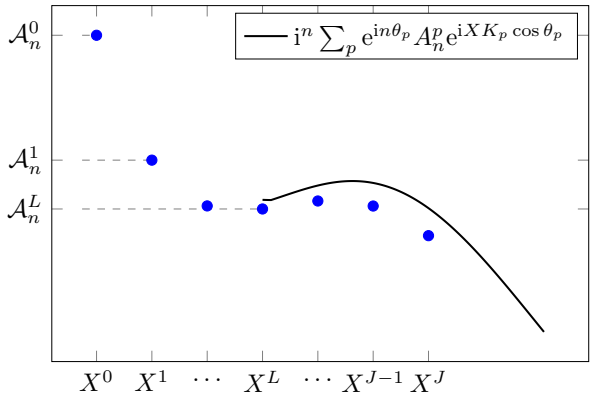

FIG. 3. *An illustration of the discrete solution $\mathcal{A}^j_n$ (4.2) (blue circles) and the effective waves (3.8) (black line). We restrict the coefficients A^p_n of the effective waves by imposing that the black line passes close to the $\mathcal{A}^j_n$ (i.e., satisfying the matching condition (5.10)) for $X = X^L, \ldots, X^J$, where we chose $\bar{X} = X^L$. Increasing the number of effective waves will lead to a closer match between the discrete solution and effective waves.*

5.1. Using the effective waves to calculate (4.6), (4.7). Substituting the effective waves (3.8) into (4.6), then integrating and using (A.2), we arrive at

$$\mathcal{E}^{\ell}_{nm} = = \frac{\phi T_m}{\pi R_o^2} \mathrm{i}^{n+1} S^{J-\ell}_{n-m} \sum_{p=1}^{P} \frac{\mathrm{e}^{\mathrm{i}X^J K_p \cos\varphi_p} \mathrm{e}^{-\mathrm{i}n\varphi_p}}{K_p \cos\varphi_p + \cos\theta_{\mathrm{inc}}} A^p_n, \tag{5.1}$$

where we used $X^J - X^{\ell} = X^{J-\ell} \ge 0$ for $J \ge \ell$, when substituting $S_{n-m}(X^J - X^{\ell})$ with (A.2). Employing (3.11), we write (5.1) in matrix form

$$\sum_n \mathcal{E}^{\ell}_{nm} = (\mathbf{E}_m \boldsymbol{\alpha})_{\ell}, \quad (\mathbf{E}_m)_{\ell p} = \frac{\phi T_m}{\pi R_o^2} \sum_n \mathrm{i}^{n+1} S^{J-\ell}_{n-m} \frac{\mathrm{e}^{\mathrm{i}X^J K_p \cos\varphi_p} \mathrm{e}^{-\mathrm{i}n\varphi_p}}{K_p \cos\varphi_p + \cos\theta_{\mathrm{inc}}} a^p_n. \tag{5.2}$$

To calculate (4.7), we first discretize the integral then substitute the effective

waves (3.8), leading to

$$\mathcal{R}^{\ell}_{nm} = \chi_{\{\ell>J-q\}}\frac{\phi T_m}{\pi R_o^2}\sum_{j=J}^{\ell+q}\mathcal{A}_n(X^j)(B^{j-\ell}_{n-m} - S^{j-\ell}_{n-m})\sigma_{\ell j} \tag{5.3}$$

$$= \chi_{\{\ell>J-q\}}\frac{\phi T_m \mathrm{i}^n}{\pi R_o^2}\sum_{j=J}^{\ell+q}\sum_{p=1}^{P} A^p_n \mathrm{e}^{-\mathrm{i}n\varphi_p}\mathrm{e}^{\mathrm{i}X^j K_p\cos\varphi_p}(B^{j-\ell}_{n-m} - S^{j-\ell}_{n-m})\sigma_{\ell j},$$

where $\sigma_{\ell j}$ represents the discrete integral in the domain $[X^J, X^{\ell+q}]$. Using (3.11), just as we did in (5.2), we can write the above in matrix form

$$\sum_n \mathcal{R}^{\ell}_{nm} = (\mathbf{R}_m\boldsymbol{\alpha})_\ell. \tag{5.4}$$

We can now rewrite the integral equation (4.4), using the above equations, in the compact form

$$(\mathbf{E}_m + \mathbf{R}_m)\boldsymbol{\alpha} - \boldsymbol{I}\boldsymbol{\mathcal{A}}_m + \sum_n \boldsymbol{Q}_{mn}\boldsymbol{\mathcal{A}}_n = \boldsymbol{b}_m, \tag{5.5}$$

which is valid for all m. If $\boldsymbol{\alpha}$ were known, then we could calculate the discrete solution $\boldsymbol{\mathcal{A}}_n$ from the above. However, the $\boldsymbol{\alpha}$ also depends on the $\boldsymbol{\mathcal{A}}_n$, as we show below.

5.2. The effective waves in terms of the discrete form. The equations to determine the effective waves, so far, are (3.9) and (3.10). To calculate the integral in (3.10), we discretize and substitute (4.2), which leads to the discrete form of the extinction equation (3.10):

$$\mathbf{w}^{\mathrm{T}}\boldsymbol{\alpha} = \mathbb{G}^{\mathrm{T}}\mathbb{A} + \mathrm{i}\pi R_o^2\cos\theta_{\mathrm{inc}}, \tag{5.6}$$

where $\cdot^{\mathrm{T}}$ denotes the transpose, we used (4.3), $g(\bar{X}) = \mathbb{G}^T\mathbb{A} = \sum_n \mathbf{G}^T_n\boldsymbol{\mathcal{A}}_n$,

$$w^p = 2\phi\sum_{n=-\infty}^{\infty}\mathrm{e}^{\mathrm{i}n\theta_{\mathrm{inc}}}\mathrm{e}^{-\mathrm{i}n\varphi_p}\frac{\mathrm{e}^{\mathrm{i}(K_p\cos\varphi_p - \cos\theta_{\mathrm{inc}})X^L}}{K_p\cos\varphi_p - \cos\theta_{\mathrm{inc}}}a^p_n, \tag{5.7}$$

$$(\mathbf{G}_n)_j = 2\phi\mathrm{e}^{\mathrm{i}n\theta_{\mathrm{inc}}}(-\mathrm{i})^{n-1}\mathrm{e}^{-\mathrm{i}X^j\cos\theta_{\mathrm{inc}}}\sigma_j, \tag{5.8}$$

and as the domain of the integral in (3.10) is only up to $X^L = \bar{X} \le X^J$, we set $(\mathbf{G}_n)_j = 0$ for $j > L$.

When using P effective wavenumbers, there are P unknowns $\alpha^1, \ldots, \alpha^P$, with, so far, only one scalar equation (5.6) to determine them. To determine the α^p, we match the sum of effective waves (3.8) with the discrete form $\mathcal{A}^j_n$ in the interval: $X^L < X < X^J$, as shown in Figure 3. To do this we could enforce

$$\mathcal{A}^j_n = \mathrm{i}^n\sum_p \mathrm{e}^{-\mathrm{i}n\varphi_p}\mathrm{e}^{\mathrm{i}X^j K_p\cos\varphi_p}a^p_n\alpha^p = \boldsymbol{\alpha}^{\mathrm{T}}\mathbf{v}^j_n \quad \text{for } j = L, L+1, \ldots, J. \tag{5.9}$$

However, for $n \neq 0$ the coefficients $\mathcal{A}^j_n$ and a^p_n can be very small, and the above would not enforce the extinction equation (5.6). So rather than use (5.9) for every n, it is more robust to minimize the difference:

$$\frac{1}{J-L}\min_{\boldsymbol{\alpha}}\sum_n\sum_{j=L}^{J}|\mathcal{A}^j_n - \boldsymbol{\alpha}^{\mathrm{T}}\mathbf{v}^j_n|^2 \quad \text{subject to} \quad \mathbf{w}^{\mathrm{T}}\boldsymbol{\alpha} = \mathbb{G}^{\mathrm{T}}\mathbb{A} + \mathrm{i}\pi R_o^2\cos\theta_{\mathrm{inc}}, \tag{5.10}$$

where the constraint enforces (5.6). For details on how to solve (5.10) see section SM2. The solution to the above is

$$\boldsymbol{\alpha} = \mathbb{L}^{\mathrm{T}}\mathbb{A} + \frac{\mathrm{i}\pi R_o^2 \cos\theta_{\mathrm{inc}}}{\mathbf{w}^T\mathbf{V}^{-1}\overline{\mathbf{w}}}\mathbf{V}^{-1}\overline{\mathbf{w}}, \tag{5.11}$$

where $\overline{\mathbf{w}}$ is the conjugate of $\mathbf{w}$, and the block matrix $\mathbb{L} = [\ldots, \mathbf{L}_{-n}, \mathbf{L}_{1-n}, \ldots, \mathbf{L}_n, \ldots]$, with

$$\mathbb{L}^{\mathrm{T}}\mathbb{A} = \sum_n \mathbf{L}_n^{\mathrm{T}}\boldsymbol{\mathcal{A}}_n, \quad \mathbf{L}_n^{\mathrm{T}} = \mathbf{Z}_n^{\mathrm{T}} + w^{-1}\mathbf{V}^{-1}\overline{\mathbf{w}}(\mathbf{G}_n^{\mathrm{T}} - \mathbf{w}^{\mathrm{T}}\mathbf{Z}_n^{\mathrm{T}}), \tag{5.12}$$

$$\mathbf{V} = \sum_n \sum_{j=L}^{J} \overline{\mathbf{v}}_n^j (\mathbf{v}_n^j)^{\mathrm{T}}, \quad \mathbf{Z}_n^{\mathrm{T}} = [\mathbf{0}\cdots\mathbf{0}\,\mathbf{V}^{-1}\overline{\mathbf{v}}_n^L \cdots \mathbf{V}^{-1}\overline{\mathbf{v}}_n^J]. \tag{5.13}$$

Finally, substituting $\boldsymbol{\alpha}$ (5.11) into (5.5), we reach an equation which we can solve for $\mathbb{A}$:

$$\boxed{((\mathbb{E}+\mathbb{R})\mathbb{L}^{\mathrm{T}} + \mathbb{M})\mathbb{A} = \mathbb{B} \qquad \text{(matching method)},} \tag{5.14}$$

where $\mathbb{E}$ and $\mathbb{R}$ have components $\mathbf{E}_m$ and $\mathbf{R}_m$, given by (5.2) and (5.4), respectively, while the components of the block matrices $\mathbb{B}$ and $\mathbb{M}$ are

$$\mathbf{B}_m = \mathbf{b}_m - \frac{\mathrm{i}\pi R_o^2 \cos\theta_{\mathrm{inc}}}{\mathbf{w}^T\mathbf{V}^{-1}\overline{\mathbf{w}}}(\mathbf{E}_m + \mathbf{R}_m)\mathbf{V}^{-1}\overline{\mathbf{w}}, \tag{5.15}$$

$$\mathbf{M}_{mn} = -\delta_{mn}\mathbf{I} + \mathbf{Q}_{mn}. \tag{5.16}$$

To summarize, the terms $\mathbf{w}$, $\mathbf{V}$, and $\mathbb{L}$ are given by (5.7), (5.13), and (5.12), $\mathbf{Q}_{mn}$ is given by (4.5), and both $\mathbb{A}$ and $\mathbf{b}_m$ are given by (4.2). The angle θ_{inc} is the angle of the incident plane wave (2.7), and R_o is a nondimensional particle radius (2.21) which increases with the frequency. The block matrices $\mathbb{G}$, $\mathbb{B}$, $\mathbb{A}$, $\mathbb{E}$, $\mathbb{R}$, $\mathbb{L}$, and $\mathbb{Z}$ all have only one column. The elements of these columns are either column vectors ($\mathbf{G}_m$, $\mathbf{B}_m$, $\boldsymbol{\mathcal{A}}_m$) or matrices ($\mathbf{E}_m$, $\mathbf{R}_m$, $\mathbf{L}_m$, and $\mathbf{Z}_m$).

5.3. The matching algorithm. We can now understand how to truncate the effective wave series (3.8): assume the wavenumbers K_p are ordered so that Im K_p increases with $p = 1, \ldots, P$. Then note that the larger Im $(X^J K_p \cos\varphi_p)$ is, the less the contribution this effective wave will make to the matching (5.10), $\mathbf{w}$ (5.6), $\mathcal{R}_{nm}^{\ell}$ (5.3), and $\mathcal{E}_{nm}^{\ell}$ (5.2). That is, we can choose P such that Im $(X^J K_P \cos\varphi_P)$ is large enough so that this wave will not affect the solution $\mathbb{A}$.

To aid reproducibility, we explain how to solve (5.14), and determine $\mathbb{A}$, by using an algorithm in section SM3.

6. The resulting methods. Here we summarize the matching method and other methods for solving (4.1). To differentiate between results for the different methods we use the superscripts M, D, and O. That is, we denote the field $\mathcal{A}_n(X)$ as

$$\mathcal{A}_n^M(X) \quad \text{(matching method)}, \quad \mathcal{A}_n^D(X) \quad \text{(discrete method)}, \tag{6.1}$$

$$\mathcal{A}_n^O(X) \quad \text{(one-effective-wave method)}. \tag{6.2}$$

For the matching method, we solve (5.14) to obtain

$$\boxed{\mathcal{A}_n^M(X) = \begin{cases} \mathcal{A}_n^j = (\boldsymbol{\mathcal{A}}_n)_j, & X = X^j, \\ \mathrm{i}^n \sum_{p=1}^{P} \mathrm{e}^{-\mathrm{i}n\varphi_p} \mathrm{e}^{\mathrm{i}XK_p\cos\varphi_p} a_n^p \alpha^p, & X > X^J \end{cases} \text{(matching method)},} \tag{6.3}$$

where the α^p are given from (5.11), and φ_p, K_p, and a_n^p are solutions to (3.2, 3.9, 3.11). For details on the matching method, see Algorithm SM3.1 in the supplementary material.

The one-effective-wave method is the typical method used in the literature. It consists in using only one effective wavenumber K_1, that is, (3.1) with $p = 1$. This one wavenumber K_1 is often given explicitly in terms of either a low-volume-fraction or a low-frequency expansion. However, as we explore both moderate-frequency and moderate volume fractions, we will instead numerically solve for K_1, the least attenuating wavenumber. To solve for K_1 and A_n^1 we take $\bar{X} = 0$ and numerically solve (3.9) and (3.10) for $P = p = 1$. The Snell angle φ_1 is determined from (3.2), with $K = K_1$ and $\varphi = \varphi_1$. The result is

$$\boxed{\mathcal{A}_n^O(X) = \mathrm{i}^n \mathrm{e}^{-\mathrm{i}n\varphi_1} \mathrm{e}^{\mathrm{i}XK_1\cos\varphi_1} A_n^1 \quad \text{(one-effective-wave method).}} \tag{6.4}$$

From subsection 4.1, we can devise a purely numerical method, which requires a much larger meshed domain for X. The resulting field is

$$\boxed{\mathcal{A}_n^D(X^j) = \begin{cases} (\mathbb{A}_n^D)^j, & j \le J, \\ 0, & j > J \end{cases} \quad \text{(discrete method).}} \tag{6.5}$$

This discrete method gives a solution for a material occupying the layer $0 < X < X^J$ and $Y \in \mathbb{R}$. If the layer is deep enough and the wave decays fast enough, then this discrete method will be the solution for an infinite half-space. Algorithm SM3.1 in the supplementary material can be used to calculate this discrete method by taking $P = 1$, $J = L$ instead of step 7, as there is no matching region, and replacing steps 9–15 with: solve for $\mathbb{A}$ by using $\mathbb{M}\mathbb{A}^D = \mathbb{B}$ instead of (5.14).

6.1. Reflection coefficient. The reflection coefficient $\mathfrak{R}$ is the key information required for many measurement techniques. We can compare the different methods for calculating the average wave by comparing their resulting reflection coefficient, which is much simpler than comparing the resulting fields $\mathcal{A}_n(X)$.

Consider a particulate material occupying the region $x > 0$, and choose a point (x, y) to measure the reflection, with $x < 0$; then the ensemble average reflection coefficient $\mathfrak{R}$ is such that

$$\langle u(x,y)\rangle = u_{\mathrm{inc}}(x,y) + \mathfrak{R}\mathrm{e}^{\mathrm{i}k(-x\cos\theta_{\mathrm{inc}} + y\sin\theta_{\mathrm{inc}})}. \tag{6.6}$$

By combining (2.17)–(2.19), we conclude that

$$\mathfrak{R} = \frac{\phi}{\pi R_o^2} \mathrm{e}^{\mathrm{i}X\cos\theta_{\mathrm{inc}}} \sum_n \int_0^\infty \mathcal{A}_n(X_1) \int_{-\infty}^\infty \mathrm{e}^{\mathrm{i}Y_0\sin\theta_{\mathrm{inc}}} F_n(\mathbf{X}_0)\, dY_0\, dX_1, \tag{6.7}$$

where we used $\mathbf{X}_0 = \mathbf{X}_1 - \mathbf{X}$ and the nondimensional parameters (2.21). The integral in Y_0 is given by (A.2), which, noting that $X_0 > 0$, leads to

$$\mathfrak{R} = \frac{2\phi}{\pi R_o^2 \cos\theta_{\mathrm{inc}}} \sum_n \mathrm{i}^n \mathrm{e}^{-\mathrm{i}n\theta_{\mathrm{inc}}} \int_0^\infty \mathcal{A}_n(X_1) \mathrm{e}^{\mathrm{i}X_1\cos\theta_{\mathrm{inc}}} dX_1. \tag{6.8}$$

Substituting the matching method field (6.3) into (6.8) leads to

(6.9)
$$\boxed{\begin{aligned}\mathfrak{R}^M = &\sum_{n=-\infty}^{\infty} \frac{2\phi}{\pi R_o^2 \cos\theta_{\text{inc}}} \qquad \text{(matching method)}\\ &\times \left[\mathrm{i}^n \sum_{j=0}^{J} \sigma_j \mathcal{A}_n^j \mathrm{e}^{\mathrm{i}X^j \cos\theta_{\text{inc}} - \mathrm{i}n\theta_{\text{inc}}} + \mathrm{i} \sum_{p=1}^{P} \alpha^p a_n^p \mathrm{e}^{\mathrm{i}n\varphi_{\text{ref}}^p} \frac{\mathrm{e}^{\mathrm{i}X^J(K_p \cos\varphi_p + \cos\theta_{\text{inc}})}}{K_p \cos\varphi_p + \cos\theta_{\text{inc}}} \right],\end{aligned}}$$

where $\varphi_{\text{ref}}^p = \pi - \theta_{\text{inc}} - \varphi_p$. For an interpretation of the reflection angle φ_{ref}^p, see [21, Figure 7].

For the discrete method, we discretize (6.8), which leads to

(6.10)
$$\boxed{\mathfrak{R}^D = \sum_{n=-\infty}^{\infty} \frac{2\phi}{\pi R_o^2 \cos\theta_{\text{inc}}} \mathrm{i}^n \sum_{j=0}^{J} \sigma_j \mathcal{A}_n^j \mathrm{e}^{\mathrm{i}X^j \cos\theta_{\text{inc}} - \mathrm{i}n\theta_{\text{inc}}} \quad \text{(discrete method).}}$$

Alternatively, to obtain the reflection coefficient for one effective wave (6.4), we set $J = 0$ and $P = 1$ in (6.9) to reach

(6.11)
$$\boxed{\mathfrak{R}^O = \sum_{n=-\infty}^{\infty} \frac{2\phi}{\pi R_o^2 \cos\theta_{\text{inc}}} \frac{\mathrm{i}A_n^1 \mathrm{e}^{\mathrm{i}n\varphi_{\text{ref}}^1}}{K_1 \cos\varphi_1 + \cos\theta_{\text{inc}}} \quad \text{(one-effective-wave method),}}$$

which agrees with equations (41) and (42) from [32], when expanding for low volume fraction ϕ.

7. Numerical experiments. For simplicity, we consider circular particles (2.6) for all numerical experiments, in which case, the nondimensional radius (2.21) $R_o = a_o k$, where a_o is the particle radius.

For the material properties we use a background material filled with particles which either strongly or weakly scatter the incident wave. These are given, respectively, by

(7.1)
$$\frac{c_o}{c} = 0.5, \quad \frac{\rho_o}{\rho} = 0.5 \qquad \text{(strong scatterers),}$$

(7.2)
$$\frac{c_o}{c} = 1.1, \quad \frac{\rho_o}{\rho} = 8.0 \qquad \text{(weak scatterers),}$$

noting that $\rho_o \gg \rho$ leads to weaker scattering than $\rho_o \ll \rho$. We will use a range of angles of incidence θ_{inc}, particle volume fractions ϕ, and particle radiuses R_o, which is equivalent to varying the incident wavenumbers k.

7.1. Comparing the fields. Figure 4 shows several examples of $\mathcal{A}_n^M$ from (6.3). As a comparison we have shown the one-effective-wave field $\mathcal{A}_n^O$ (6.4) as well. To not clutter the figure, we have not shown the discrete field $\mathcal{A}_n^D$ (6.5), which would lie exactly on top of $\mathcal{A}_n^M$. Figure 4 reveals how the discrete and effective wave parts of $\mathcal{A}_n^M$ very closely overlap in the matching region $X^L \le X \le X^J$. This close overlap is not due to overfitting, as there are more than double the number of equations than unknowns.

We now look closely at a specific case: particle volume fraction $\phi = 20\%$ and nondimensional particle radius $R_o = 0.4$ for the strong scatterers (7.1). Figure 5

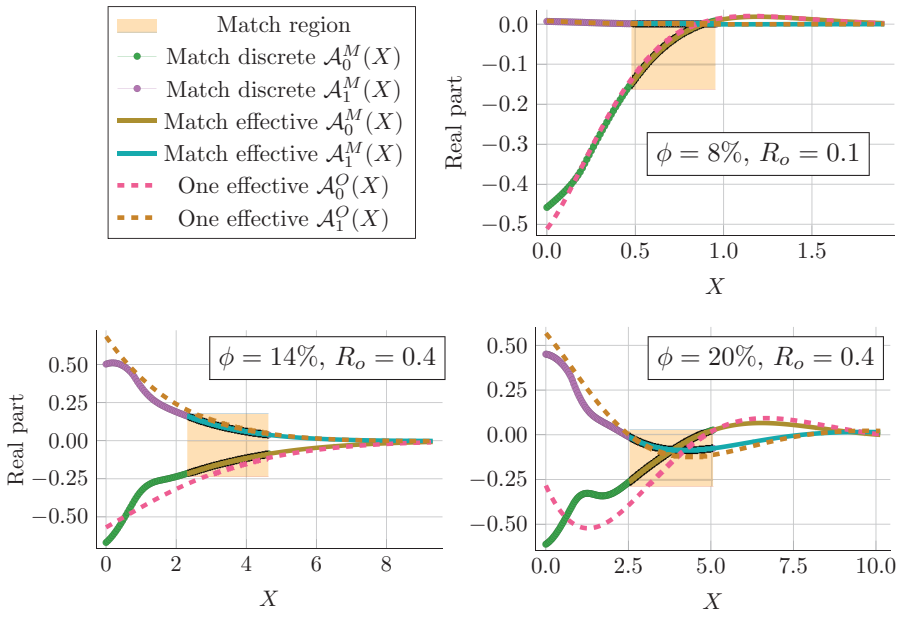

FIG. 4. *These graphs show the matching field* (6.3) *and the one-effective-wave field* (6.4) *for a material with circular particles, incident wave angle* $\theta_{\text{inc}} = 0$*, and properties* (7.1)*. The nondimensional radius* $R_o = ka_o$ *and volume fraction* ϕ *are shown on each graph. We used six effective wavenumbers* ($P = 6$) *for the bottom two graphs, and four effective wavenumbers* ($P = 4$) *for the top right graph. Note that the discrete and effective parts of the matching fields overlap in the match region. The one-effective-wave field in general loses accuracy close to the interface* $X = 0$*, which is why it gives inaccurate predictions for the reflection coefficient* $\mathcal{R}^O$ (6.11).

shows the effective wavenumbers used and how the greater the attenuation Im K_p is, the lower the resulting amplitude $|\alpha^P|$ of the effective wave is, and therefore the less it contributes to the total transmitted wave. We also see in Figure 5(c) how increasing the number of effective waves (while fixing everything else) results in a smaller difference between the fields of the matching and discrete methods. This clearly confirms that the field $\mathcal{A}_n$ is composed of these multiple effective waves. Figure 6 shows how the matching method (6.3) and the discrete method (6.5) closely overlap with

$$\max_{X,n} \|\mathcal{A}_n^M(X) - \mathcal{A}_n^D(X)\| = 4.5 \times 10^{-4},$$

which is similar to the matching error 4.7×10^{-5} given by the sum $(5.10)_1$. The dotted and dashed curves in Figure 6 demonstrate how the matching method is only accurate when using the effective wavenumbers that satisfy (3.9). This agreement between the matching and discrete methods is not isolated to specific material properties and frequencies; we have yet to find a case where the two methods do not show excellent agreement.[6] Further, when increasing the number of effective wavenumbers P and lowering the tolerance *tol* in Algorithm SM3.1, the two methods converge to the same solution, as indicated by Figure 5(c). In this paper we will not explore this convergence in detail, but we will show that the two methods produce the same reflection coefficient for a large parameter range.

[6]Naturally, when the truncation error of the discrete method is very large, we found that the result did not agree with the matching method. Note that the truncation error of the discrete method is large when $\mathcal{A}_n(X)$ is weakly attenuating as X increases.

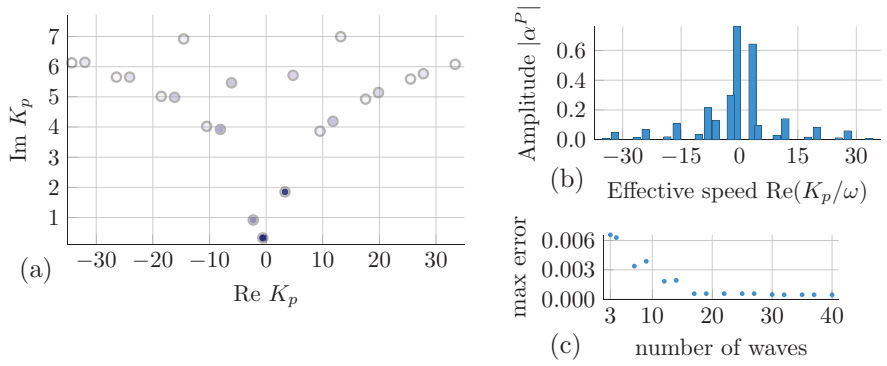

FIG. 5. *These graphs show the influence of the effective wavenumbers for the strong scatterers* (7.1) *with particle volume fraction* $\phi = 20\%$, *nondimensional radius* $R_o = 0.4$, *and incident wave angle* $\theta_{\mathrm{inc}} = 0.4$. *The resulting field* $\mathcal{A}_n^M$ *is shown in Figure* (6). (a) *shows the effective wavenumbers, with each marker corresponding to one wavenumber* K_P *whose color darkens as the amplitude of its wave field* α^P *increases. Clearly the larger the attenuation* $\mathrm{Im}\, K_p$, *the lower the amplitude* α^P. (b) *reveals how the amplitude* α^P *decreases when the effective phase speed increases in magnitude.* (c) *shows how the maximum error between the fields of the matching and discrete methods decreases when increasing the number of effective waves used by the matching method. Note: if we had not included the three lowest attenuating wavenumbers, the maximum error would be larger than* 0.17.

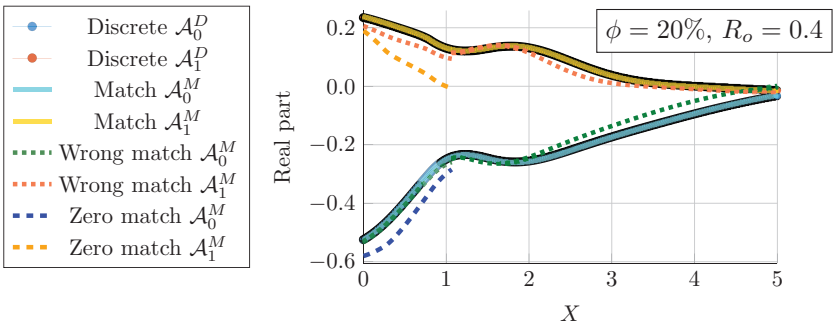

FIG. 6. *This graph shows that the matching method* (6.3) *overlaps with the discrete method* (6.5) *(a purely numerical method). The effective wavenumbers used are shown in Figure* 5, *and the material properties are given by* (7.1). *The dashed and dotted curves also result from the matching method but use the wrong effective waves: the dotted curve wrong match* $\mathcal{A}_0^M$ *and* $\mathcal{A}_1^M$ *use the effective wavenumbers* (3.9) *multiplied by* 1.2. *The zero match fields zero all the effective wave amplitudes* $a_n^p = 0$ *and* $\mathcal{A}_n^M(X) = 0$ *for* $X > 1$.

7.2. Comparing reflection coefficients. The reflection coefficient $\mathfrak{R}$ is a simple way to compare the different methods in section 6. Many scattering experiments aim to estimate $\mathfrak{R}$ [67, 66]. The accuracy of estimating $\mathfrak{R}$ is also directly related to the accuracy of calculating the transmitted waves.

In Figure 7 we compare the reflection coefficient for the discrete method $\mathfrak{R}^D$ (6.10), matching method $\mathfrak{R}^M$ (6.9), and two methods that use only one effective wavenumber (6.11): the *one effective* $\mathfrak{R}^O$ uses a numerical solution for K_1 (the wavenumber with the smallest imaginary part), while the *low vol. frac* $\mathfrak{R}^O$ uses a low-volume-fraction expansion for the wavenumber [32].

In Figure 7(a) we compare the reflection coefficients for strong scatterers (7.1) when varying the particle radius R_o (or likewise varying the wavenumber k) with a fixed volume fraction $\phi = 20\%$. We use at most 1600 points for the X mesh and fewer

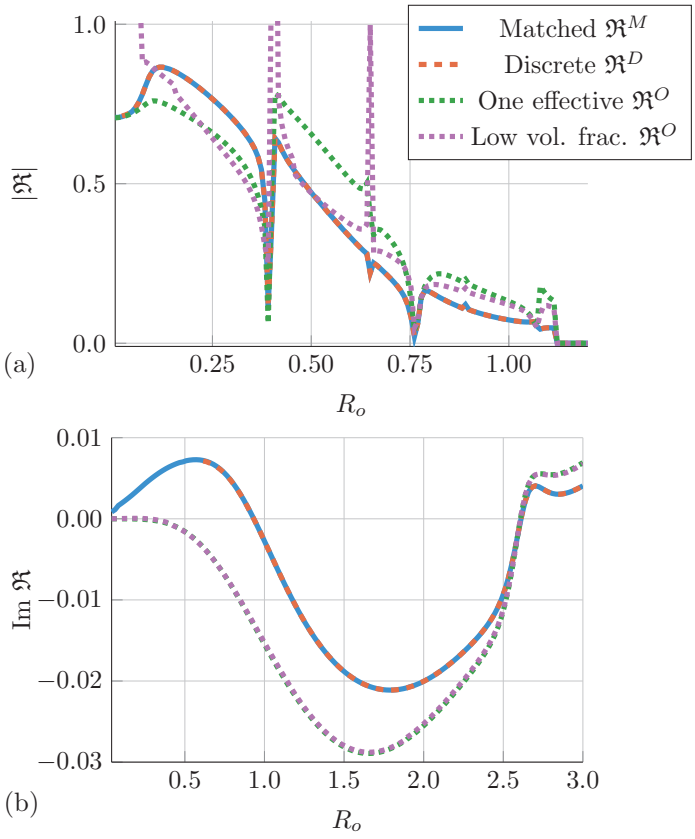

FIG. 7. *The reflection coefficients from the methods in section* 6 *as a function of the nondimensional particle radius* R_o*:* (a) *has strong scattering particles* (7.1) *with* $\phi = 20\%$ *and* $\theta_{\text{inc}} = 0.0$*, while* (b) *has weak scattering particles* (7.2) *with* $\phi = 25\%$ *and* $\theta_{\text{inc}} = 0.4$*. Note that the one-effective-wave fields almost overlap in this case. The real part of the curves in* (b) *are even closer together, with* $\max_{R_o} |\text{Re}(\mathfrak{R}^O - \mathfrak{R}^M)| = 0.0026$ *for the one effective* $\mathfrak{R}^O$*.*

than 100 points for the X mesh of the matching method, and aim for a tolerance of 10^{-5} for the fields.

We clearly see that $\mathfrak{R}^D$ and $\mathfrak{R}^M$ (6.9) overlap. For $R_o > 0.03$ the maximum difference $\max_{R_o} |\mathfrak{R}^M - \mathfrak{R}^D| < 0.0014$. For $R_o < 0.03$ we have not shown $\mathfrak{R}^D$ because the numerical truncation error became too large (compared to our tolerance). This occurs when the fields $\mathcal{A}^D(X)$ decay slowly, which occurs for small particles (or low frequency). However, for low frequency the one effective $\mathfrak{R}^O$ is asymptotically accurate [44], and we see that $\mathfrak{R}^M$ does converge to $\mathfrak{R}^O$ as $R_o \to 0$. However, for larger R_o the error of the one effective $\mathfrak{R}^O$ is as much as 20%, while the low vol. frac. $\mathfrak{R}^O$ commits even larger errors. These larger errors are not unexpected, because the accuracy of the low-volume-fraction expansion depends on the type of scatterers and frequency [44], and can diverge in the limit $R_o \to 0$ [20].

Figure 7(b) compares the reflection coefficients for weak scatterers (7.2). We use at most 2200 points for the X mesh and fewer than 100 points for the X mesh of the matching method, and aim for a tolerance of 10^{-5} for the fields.

Again, as before, we do not show $\mathfrak{R}^D$ for values of R_o where the numerical truncation error become large (relative to our tolerance). For this case of weak scatterers we

see that the difference between the methods is less, though the reflection coefficient is also smaller with mean $|\mathfrak{R}^M| = 0.058$. Still, the relative error of Im $(\mathfrak{R}^M - \mathfrak{R}^O) \approx 10\%$. The imaginary part of the reflection coefficient, and where it changes sign, can be key for characterizing random microstructure [48]. The real part of the reflection coefficients is not shown, as the relative errors for the real part are even smaller.

8. Conclusions. Our overriding message is that there is not one, but a series of waves, with different effective wavenumbers, that propagate (with attenuation) in an ensemble-averaged random particulate material. These waves must be included to accurately calculate reflection and transmission. Figure 2 shows examples of these effective wavenumbers.

Although there is an analytic proof [18] that there exist a series of effective waves, which solve (2.20), this current paper shows how to calculate these by using a matching method (6.3). In our numerical experiments in section 7, we show that the matching method converges to a numerical solution (the discrete method) for a broad range of wavenumbers k (or equivalently the nondimensional radius R_o), particle volume fractions, and two sets of material properties. For example, Figure 6 compares the average fields $\mathcal{A}_n(X)$, and Figure 7 the reflection coefficients $\mathfrak{R}$ of the matching and discrete methods. The drawback of the discrete method (6.5) is that it is computationally intensive, especially for low wave attenuation, requiring a spatial mesh between 1600 and 2000 elements to reach the same tolerance as the matching method, which used only 100 elements.

For small incident wavenumbers k, the matching method converges to a result which assumes there exists only one effective wave for both strong and weak scatterers. Qualitatively, the fields $\mathcal{A}_n(X)$ from the one-effective-wave (6.4) and matching (6.3) methods agreed well when moving away from the material's interface; for example, see Figure 4. However, as the fields are not the same near the interface, the resulting reflection coefficients can significantly differ, as shown in Figure 7.

8.1. The next steps. Here we comment on a few directions for future work. One important limit, which we did not investigate here, is the low volume fraction limit: $\phi \ll 1$. In numerical experiments, not reported here, we found that the matching method converges to the one-effective-wave method in the limit for low ϕ. It appears that as ϕ decreases the Im K_p, for $p > 2$, tends to $+\infty$, implying that the boundary layer $\bar{X}$ shrinks and makes all but K_1 insignificant. This limit deserves a detailed analytic investigation in a separate paper.

The consequences of this work have a direct impact on effective wave methods used for acoustic, elastic, electromagnetic, and even quantum wave scattering. That said, many of these fields use vector wave equations and require the average intensity. So one challenge is to translate the results of this paper to vector wave equations and the average intensity. Note that for electromagnetic waves, much of the groundwork for the average fields has already been done [23, 24].

The radiative transfer equations are one outcome of properly deducing the averaged intensity for waves in particulate materials. For example, for electromagnetic waves, radiative transfer equations have been deduced under assumptions such as weak scattering, sparse particle volume fractions, and one effective wavenumber K_1 [37]. Within the confines of the assumptions used, radiative transfer methods (and modifications) are leading to accurate predictions of the reflected intensity [41, 65, 47]. We speculate that this work will eventually lead to accurate predictions for reflected intensity for a broad range of frequencies and particle properties.

Data and reproducibility. All results can be reproduced with the publicly available software [17], which has examples on how to calculate the effective wavenumbers and the matching method, as well as the finite-difference method that we present.

Appendix A. Wiener–Hopf kernel. Here we reduce (2.20) to the Wiener–Hopf equation (4.1). First we separate the double integral:

$$\int_{\substack{x_2>0\\ \|\mathbf{x}_2-\mathbf{x}_1\|>a_{12}}} \mathcal{A}_n(kx_2)\mathrm{e}^{\mathrm{i}(y_2-y_1)k\sin\theta_{\mathrm{inc}}}F_{n-m}(k\mathbf{x}_2-k\mathbf{x}_1)\mathrm{d}\mathbf{x}_2 = \frac{1}{k^2}\int_{x_2>0}\mathcal{A}_n(X_2)\int_{Y^2>R_o^2\gamma^2-X^2}\mathrm{e}^{\mathrm{i}Y\sin\theta_{\mathrm{inc}}}F_{n-m}(\mathbf{X})\mathrm{d}Y\,\mathrm{d}X,$$

where we used $\mathbf{X}=k\mathbf{x}_2-k\mathbf{x}_1$ and the parameters (2.21). We can then rewrite

$$\text{(A.1)}\quad \int_{Y^2>R_o^2\gamma^2-X^2}\mathrm{e}^{\mathrm{i}Y\sin\theta_{\mathrm{inc}}}F_{n-m}(\mathbf{X})\mathrm{d}Y = \chi_{\{|X|<R_o\gamma\}}B_{n-m}(X)+\chi_{\{|X|>R_o\gamma\}}S_{n-m}(X),$$

where $\chi_{\{\mathrm{true}\}}=1$ and $\chi_{\{\mathrm{false}\}}=0$. From [32, eq. (37)] we have

(A.2)
$$S_n(X)=\int_{-\infty}^{\infty}\mathrm{e}^{\mathrm{i}Y\sin\theta_{\mathrm{inc}}}F_n(\mathbf{X})\mathrm{d}Y=\frac{2}{\cos\theta_{\mathrm{inc}}}\begin{cases}\mathrm{i}^n\mathrm{e}^{-\mathrm{i}n\theta_{\mathrm{inc}}}\mathrm{e}^{\mathrm{i}X\cos\theta_{\mathrm{inc}}}, & X\geq 0,\\ (-\mathrm{i})^n\mathrm{e}^{\mathrm{i}n\theta_{\mathrm{inc}}}\mathrm{e}^{-\mathrm{i}X\cos\theta_{\mathrm{inc}}}, & X<0.\end{cases}$$

The $B_{n-m}(X)$ in (A.1) only need to be evaluated for a small portion of the domain of X, and are given by

$$\text{(A.3)}\quad B_n(X)=\int_{-\infty}^{\infty}\chi_{\{Y^2>R_o^2\gamma^2-X^2\}}\mathrm{e}^{\mathrm{i}Y\sin\theta_{\mathrm{inc}}}F_n(\mathbf{X})\mathrm{d}Y = 2(-1)^n\int_{\sqrt{R_o^2\gamma^2-X^2}}^{\infty}\cos\left(Y\sin\theta_{\mathrm{inc}}+n\Theta\right)H_n(R)\mathrm{d}Y.$$

Because the integrand tends to zero slowly as Y increases, we use an asymptotic approximation to evaluate the integral, namely,

$$\text{(A.4)}\qquad \cos\left(Y\sin\theta_{\mathrm{inc}}+n\Theta\right)=\cos((n\pi)/2+Y\sin(\theta_{\mathrm{inc}}))+\mathcal{O}(X/Y),$$

$$\text{(A.5)}\qquad H_n(R)=-(-1)^{3/4}\mathrm{e}^{-\mathrm{i}n\pi/2}\sqrt{\frac{2}{\pi Y}}+\mathcal{O}(X^{3/2}/Y^{3/2}),$$

to rewrite

$$\text{(A.6)}\quad B_n(X)=2(-1)^n\int_{\sqrt{R_o^2\gamma^2-X^2}}^{Y_1}\cos\left(Y\sin\theta_{\mathrm{inc}}+n\Theta\right)H_n(R)\mathrm{d}Y + \frac{(1+\mathrm{i})\mathrm{e}^{\mathrm{i}Y_1(1-\sin\theta_{\mathrm{inc}})}}{\sqrt{\pi Y_1}\cos^2\theta_{\mathrm{inc}}}\left[(-1)^n\mathrm{e}^{2\mathrm{i}Y_1\sin\theta_{\mathrm{inc}}}(1-\sin\theta_{\mathrm{inc}})+1+\sin\theta_{\mathrm{inc}}\right]+\mathcal{O}(X/Y_1).$$

Then as X is bounded by $|X|<R_o\gamma$, we can choose Y_1 such that X/Y_1 is below a prescribed tolerance.

Substituting (A.1), (A.2), (A.6) into (2.20) leads to the Wiener–Hopf integral equation (4.1).

REFERENCES

[1] M. Abramowitz and I. A. Stegun, eds., *Handbook of Mathematical Functions*, Dover, New York, 1965.

[2] G. Adomian, *The closure approximation in the hierarchy equations*, J. Stat. Phys., 3 (1971), pp. 127–133, https://doi.org/10.1007/BF01019846.

[3] G. Adomian and K. Malakian, *Closure approximation error in the mean solution of stochastic differential equations by the hierarchy method*, J. Stat. Phys., 21 (1979), pp. 181–189, https://doi.org/10.1007/BF01008697.

[4] T. Arens, S. N. Chandler-Wilde, and K. O. Haseloh, *Solvability and spectral properties of integral equations on the real line:* II. L^p*-spaces and applications*, J. Integral Equations Appl., 15 (2003), pp. 1–35.

[5] C. Arístégui and Y. C. Angel, *Effective material properties for shear-horizontal acoustic waves in fiber composites*, Phys. Rev. E, 75 (2007), 056607, https://doi.org/10.1103/PhysRevE.75.056607.

[6] L. G. Bennetts and M. A. Peter, *Spectral analysis of wave propagation through rows of scatterers via random sampling and a coherent potential approximation*, SIAM J. Appl. Math., 73 (2013), pp. 1613–1633, https://doi.org/10.1137/120903439.

[7] L. G. Bennetts, M. A. Peter, and H. Chung, *Absence of localisation in ocean wave interactions with a rough seabed in intermediate water depth*, Quart. J. Mech. Appl. Math., 68 (2015), pp. 97–113, https://doi.org/10.1093/qjmam/hbu024.

[8] S. K. Bose and A. K. Mal, *Longitudinal shear waves in a fiber-reinforced composite*, Internat. J. Solids Structures, 9 (1973), pp. 1075–1085.

[9] M. Chekroun, L. Le Marrec, B. Lombard, and J. Piraux, *Time-domain numerical simulations of multiple scattering to extract elastic effective wavenumbers*, Waves Random Complex Media, 22 (2012), pp. 398–422, https://doi.org/10.1080/17455030.2012.704432.

[10] J.-M. Conoir and A. N. Norris, *Effective wavenumbers and reflection coefficients for an elastic medium containing random configurations of cylindrical scatterers*, Wave Motion, 47 (2010), pp. 183–197, https://doi.org/10.1016/j.wavemoti.2009.09.004.

[11] F. de Hoog and I. H. Sloan, *The finite-section approximation for integral equations on the half-line*, J. Austral. Math. Soc. Ser. B, 28 (1987), pp. 415–434, https://doi.org/10.1017/S0334270000005506.

[12] J. Dubois, C. Arístégui, O. Poncelet, and A. L. Shuvalov, *Coherent acoustic response of a screen containing a random distribution of scatterers: Comparison between different approaches*, J. Phys. Conf. Ser., 269 (2011), 012004, https://doi.org/10.1088/1742-6596/269/1/012004.

[13] J. G. Fikioris and P. C. Waterman, *Multiple scattering of waves.* II. *"Hole corrections" in the scalar case*, J. Math. Phys., 5 (1964), pp. 1413–1420, https://doi.org/10.1063/1.1704077.

[14] L. L. Foldy, *The multiple scattering of waves.* I. *General theory of isotropic scattering by randomly distributed scatterers*, Phys. Rev. (2), 67 (1945), pp. 107–119.

[15] M. Ganesh and S. C. Hawkins, *A far-field based T-matrix method for two dimensional obstacle scattering*, ANZIAM J., 51 (2009), pp. C215–C230.

[16] M. Ganesh and S. C. Hawkins, *Algorithm* 975: *TMATROM—A T-matrix reduced order model software*, ACM Trans. Math. Software, 44 (2017), 9, https://doi.org/10.1145/3054945.

[17] A. L. Gower, *EffectiveWaves.jl: A package to calculate ensemble averaged waves in heterogeneous materials*, https://github.com/arturgower/EffectiveWaves.jl/tree/v0.2.0 (accessed 2018-24-10).

[18] A. L. Gower, I. D. Abrahams, and W. J. Parnell, *A Proof that Multiple Waves Propagate in Ensemble-Averaged Particulate Materials*, preprint, https://arxiv.org/abs/1905.06996, 2019.

[19] A. L. Gower and J. Deakin, *MultipleScattering.jl: A Julia library for simulating, processing, and plotting multiple scattering of waves*, https://github.com/jondea/MultipleScattering.jl (accessed 2017-12-29).

[20] A. L. Gower, R. M. Gower, J. Deakin, W. J. Parnell, and I. D. Abrahams, *Characterising particulate random media from near-surface backscattering: A machine learning approach to predict particle size and concentration*, EPL, 122 (2018), 54001.

[21] A. L. Gower, M. J. A. Smith, W. J. Parnell, and I. D. Abrahams, *Reflection from a multi-species material and its transmitted effective wavenumber*, Proc. A, 474 (2018), 20170864, https://doi.org/10.1098/rspa.2017.0864.

[22] M. Gustavsson, G. Kristensson, and N. Wellander, *Multiple scattering by a collection of randomly located obstacles—Numerical implementation of the coherent fields*, J. Quant.

Spectrosc. Radiat. Transfer, 185 (2016), pp. 95–100, https://doi.org/10.1016/j.jqsrt.2016.08.018.

[23] G. Kristensson, *Coherent scattering by a collection of randomly located obstacles—An alternative integral equation formulation*, J. Quant. Spectrosc. Radiat. Transfer, 164 (2015), pp. 97–108, https://doi.org/10.1016/j.jqsrt.2015.06.004.

[24] G. Kristensson, *Evaluation of some integrals relevant to multiple scattering by randomly distributed obstacles*, J. Math. Anal. Appl., 432 (2015), pp. 324–337, https://doi.org/10.1016/j.jmaa.2015.06.047.

[25] M. Lax, *Multiple scattering of waves*, Rev. Modern Phys., 23 (1951), pp. 287–310, https://doi.org/10.1103/RevModPhys.23.287.

[26] M. Lax, *Multiple scattering of waves.* II. *The effective field in dense systems*, Phys. Rev., 85 (1952), pp. 621–629, https://doi.org/10.1103/PhysRev.85.621.

[27] C. Layman, N. S. Murthy, R.-B. Yang, and J. Wu, *The interaction of ultrasound with particulate composites*, J. Acoust. Soc. Am., 119 (2006), pp. 1449–1456, https://doi.org/10.1121/1.2161450.

[28] C. M. Linton and P. A. Martin, *Multiple scattering by random configurations of circular cylinders: Second-order corrections for the effective wavenumber*, J. Acoust. Soc. Am., 117 (2005), pp. 3413–3423, https://doi.org/10.1121/1.1904270.

[29] C. M. Linton and P. A. Martin, *Multiple scattering by multiple spheres: A new proof of the Lloyd–Berry formula for the effective wavenumber*, SIAM J. Appl. Math., 66 (2006), pp. 1649–1668, https://doi.org/10.1137/050636401.

[30] P. Lloyd and M. V. Berry, *Wave propagation through an assembly of spheres:* IV. *Relations between different multiple scattering theories*, Proc. Phys. Soc., 91 (1967), pp. 678–688, https://doi.org/10.1088/0370-1328/91/3/321.

[31] P. A. Martin, *Multiple Scattering: Interaction of Time-Harmonic Waves with N Obstacles*, Cambridge University Press, Cambridge, 2006, https://doi.org/10.1017/CBO9780511735110.

[32] P. A. Martin, *Multiple scattering by random configurations of circular cylinders: Reflection, transmission, and effective interface conditions*, J. Acoust. Soc. Am., 129 (2011), pp. 1685–1695, https://doi.org/10.1121/1.3546098.

[33] P. A. Martin and A. Maurel, *Multiple scattering by random configurations of circular cylinders: Weak scattering without closure assumptions*, Wave Motion, 45 (2008), pp. 865–880, https://doi.org/10.1016/j.wavemoti.2008.03.004.

[34] P. A. Martin, A. Maurel, and W. J. Parnell, *Estimating the dynamic effective mass density of random composites*, J. Acoust. Soc. Am., 128 (2010), pp. 571–577, https://doi.org/10.1121/1.3458849.

[35] M. I. Mishchenko, *Vector radiative transfer equation for arbitrarily shaped and arbitrarily oriented particles: A microphysical derivation from statistical electromagnetics*, Appl. Optics, 41 (2002), pp. 7114–7134, https://doi.org/10.1364/AO.41.007114.

[36] M. I. Mishchenko, *Multiple scattering, radiative transfer, and weak localization in discrete random media: Unified microphysical approach*, Rev. Geophys., 46 (2008), RG2003, https://doi.org/10.1029/2007RG000230.

[37] M. I. Mishchenko, J. M. Dlugach, M. A. Yurkin, L. Bi, B. Cairns, L. Liu, R. L. Panetta, L. D. Travis, P. Yang, and N. T. Zakharova, *First-principles modeling of electromagnetic scattering by discrete and discretely heterogeneous random media*, Phys. Rep., 632 (2016), pp. 1–75, https://doi.org/10.1016/j.physrep.2016.04.002.

[38] M. I. Mishchenko, L. D. Travis, and A. A. Lacis, *Multiple Scattering of Light by Particles: Radiative Transfer and Coherent Backscattering*, Cambridge University Press, 2006.

[39] M. I. Mishchenko, L. D. Travis, and D. W. Mackowski, *T-matrix computations of light scattering by nonspherical particles: A review*, J. Quant. Spectrosc. Radiat. Transfer, 55 (1996), pp. 535–575, https://doi.org/10.1016/0022-4073(96)00002-7.

[40] F. Montiel, V. A. Squire, and L. G. Bennetts, *Evolution of directional wave spectra through finite regular and randomly perturbed arrays of scatterers*, SIAM J. Appl. Math., 75 (2015), pp. 630–651, https://doi.org/10.1137/140973906.

[41] K. Muinonen, M. I. Mishchenko, J. M. Dlugach, E. Zubko, A. Penttilä, and G. Videen, *Coherent backscattering verified numerically for a finite volume of spherical particles*, Astrophys. J., 760 (2012), 118, https://doi.org/10.1088/0004-637X/760/2/118.

[42] A. N. Norris, *Scattering of elastic waves by spherical inclusions with applications to low frequency wave propagation in composites*, Internat. J. Engrg. Sci., 24 (1986), pp. 1271–1282, https://doi.org/10.1016/0020-7225(86)90056-X.

[43] A. N. Norris, F. Lupp, and J.-M. Conoir, *Effective wave numbers for thermo-viscoelastic media containing random configurations of spherical scatterers*, J. Acoust. Soc. Am., 131

(2012), pp. 1113–1120.
[44] W. J. Parnell and I. D. Abrahams, *Multiple point scattering to determine the effective wavenumber and effective material properties of an inhomogeneous slab*, Waves Random Complex Media, 20 (2010), pp. 678–701, https://doi.org/10.1080/17455030.2010.510858.
[45] W. J. Parnell, I. D. Abrahams, and P. R. Brazier-Smith, *Effective properties of a composite half-space: Exploring the relationship between homogenization and multiple-scattering theories*, Quart. J. Mech. Appl. Math., 63 (2010), pp. 145–175, https://doi.org/10.1093/qjmam/hbq002.
[46] V. J. Pinfield, *Thermo-elastic multiple scattering in random dispersions of spherical scatterers*, J. Acoust. Soc. Am., 136 (2014), pp. 3008–3017.
[47] J. Przybilla, M. Korn, and U. Wegler, *Radiative transfer of elastic waves versus finite difference simulations in two-dimensional random media*, J. Geophys. Res., 111 (2006), B04305, https://doi.org/10.1029/2005JB003952.
[48] R. Roncen, Z. E. A. Fellah, F. Simon, E. Piot, M. Fellah, E. Ogam, and C. Depollier, *Bayesian inference for the ultrasonic characterization of rigid porous materials using reflected waves by the first interface*, J. Acoust. Soc. Am., 144 (2018), pp. 210–221, https://doi.org/10.1121/1.5044423.
[49] S. Rupprecht, L. G. Bennetts, and M. A. Peter, *On the calculation of wave attenuation along rough strings using individual and effective fields*, Wave Motion, 85 (2019), pp. 57–66, https://doi.org/10.1016/j.wavemoti.2018.10.007.
[50] G. Sha, *Correlation of elastic wave attenuation and scattering with volumetric grain size distribution for polycrystals of statistically equiaxed grains*, Wave Motion, 83 (2018), pp. 102–110, https://doi.org/10.1016/j.wavemoti.2018.08.012.
[51] P. Sheng, *Introduction to Wave Scattering, Localization and Mesoscopic Phenomena*, Springer Ser. Materials Sci. 88, Springer-Verlag, Berlin, Heidelberg, 2006.
[52] V. P. Tishkovets, E. V. Petrova, and M. I. Mishchenko, *Scattering of electromagnetic waves by ensembles of particles and discrete random media*, J. Quant. Spectrosc. Radiat. Transfer, 112 (2011), pp. 2095–2127, https://doi.org/10.1016/j.jqsrt.2011.04.010.
[53] L. Tsang, C. T. Chen, A. T. C. Chang, J. Guo, and K. H. Ding, *Dense media radiative transfer theory based on quasicrystalline approximation with applications to passive microwave remote sensing of snow*, Radio Sci., 35 (2000), pp. 731–749, https://doi.org/10.1029/1999RS002270.
[54] L. Tsang and A. Ishimaru, *Radiative wave equations for vector electromagnetic propagation in dense nontenuous media*, J. Electromagn. Waves Appl., 1 (1987), pp. 59–72, https://doi.org/10.1163/156939387X00090.
[55] L. Tsang, J. A. Kong, and K.-H. Ding, *Scattering of Electromagnetic Waves: Theories and Applications*, John Wiley & Sons, 2004.
[56] V. Twersky, *On scattering of waves by random distributions.* I. *FreeSpace scatterer formalism*, J. Math. Phys., 3 (1962), pp. 700–715, https://doi.org/10.1063/1.1724272.
[57] V. K. Varadan, *Scattering of elastic waves by randomly distributed and oriented scatterers*, J. Acoust. Soc. Am., 65 (1979), pp. 655–657, https://doi.org/10.1121/1.382419.
[58] V. K. Varadan, V. N. Bringi, and V. V. Varadan, *Coherent electromagnetic wave propagation through randomly distributed dielectric scatterers*, Phys. Rev. D, 19 (1979), pp. 2480–2489, https://doi.org/10.1103/PhysRevD.19.2480.
[59] V. K. Varadan, V. N. Bringi, V. V. Varadan, and A. Ishimaru, *Multiple scattering theory for waves in discrete random media and comparison with experiments*, Radio Sci., 18 (1983), pp. 321–327, https://doi.org/10.1029/RS018i003p00321.
[60] V. K. Varadan, Y. Ma, and V. V. Varadan, *A multiple scattering theory for elastic wave propagation in discrete random media*, J. Acoust. Soc. Am., 77 (1985), pp. 375–385, https://doi.org/10.1121/1.391910.
[61] V. K. Varadan, V. V. Varadan, and Y.-H. Pao, *Multiple scattering of elastic waves by cylinders of arbitrary cross section.* I. *SH waves*, J. Acoust. Soc. Am., 63 (1978), pp. 1310–1319.
[62] P. C. Waterman, *Symmetry, unitarity, and geometry in electromagnetic scattering*, Phys. Rev. D, 3 (1971), pp. 825–839, https://doi.org/10.1103/PhysRevD.3.825.
[63] P. C. Waterman and R. Truell, *Multiple scattering of waves*, J. Math. Phys., 2 (1961), pp. 512–537, https://doi.org/10.1063/1.1703737.
[64] R. L. Weaver, *Diffusivity of ultrasound in polycrystals*, J. Mech. Phys. Solids, 38 (1990), pp. 55–86, https://doi.org/10.1016/0022-5096(90)90021-U.
[65] U. Wegler, M. Korn, and J. Przybilla, *Modeling full seismogram envelopes using radiative transfer theory with Born scattering coefficients*, Pure Appl. Geophys., 163 (2006), pp. 503–531, https://doi.org/10.1007/s00024-005-0027-5.

[66] R. Weser, S. Wöckel, B. Wessely, and U. Hempel, *Particle characterisation in highly concentrated dispersions using ultrasonic backscattering method*, Ultrasonics, 53 (2013), pp. 706–716, https://doi.org/10.1016/j.ultras.2012.10.013.

[67] R. West, D. Gibbs, L. Tsang, and A. K. Fung, *Comparison of optical scattering experiments and the quasi-crystalline approximation for dense media*, J. Opt. Soc. Amer. A, 11 (1994), pp. 1854–1858, https://doi.org/10.1364/JOSAA.11.001854.

[68] R.-B. Yang, *A dynamic generalized self-consistent model for wave propagation in particulate composites*, J. Appl. Mech., 70 (2003), pp. 575–582, https://doi.org/10.1115/1.1576806.